Available online at www.sciencedirect.com

ScienceDirect

Procedia Structural Integrity 13 (2018) 625–630

Structural Integrity Procedia

www.elsevier.com/locate/procedia

ECF22 - Loading and Environmental Effects on Structural Integrity

Interfacial fracture of 3D-printed bioresorbable polymers

Andrew Gleadall[a]*, Wingho Poon[b], James Allum[a], Alper Ekinci[a], Xiaoxiao Han[a], Vadim V. Silberschmidt[a]

[a]*Wolfson School of Mechanical, Electrical and Manufacturing Engineering, Loughborough University, Loughborough, LE11 3TU, UK*
[b]*Department of Materials Science and Engineering, City University of Hong Kong, 83 Tat Chee Avenue, Kowloon 999077, Hong Kong Special Administrative Region, China*

Abstract

A micro specimen for tensile testing was designed with two primary aims: (i) to characterise interface fracture behaviour between fused 3D-printed polymer filaments; and (ii) to minimise material use of high-cost medical-grade polymer since a high number of specimens are required for time-series studies (e.g. polymer degradation). Polylactide specimens were fabricated on an extrusion 3D-printer as a single-filament-wide wall. The widths of filaments were set individually, with a custom machine-control code, to achieve a higher width in the grip sections of specimens and a narrower width in their gauge section. On average, the interface between filaments was 114 μm narrower than the widest point of the filaments. Each specimen was tested in the build direction to determine the interfacial strength between 3D-printed layers. Optical microscopy was employed to characterise geometry of specimens and fracture surfaces. Samples fractured in the gauge section and the fracture surface demonstrated brittle characteristics. The specimens utilised an order of magnitude less material than ASTM D638 samples, whilst maintaining repeatability for tensile strength similar to that in other studies. The average strength was 49.4 MPa, which is comparable to data in the literature. Further optimisation of the specimen design and 3D printing strategy could realise greater reductions in material use.

Peer-review under responsibility of the ECF22 organizers.

Keywords: Additive manufacturing; 3D printing; Interface; Mechanical properties; Fracture; Micro-tensile; Medical polymers

* Corresponding author. Tel.: +44(0)-1509-227578.
E-mail address: a.gleadall@lboro.ac.uk

2452-3216
Peer-review under responsibility of the ECF22 organizers.
10.1016/j.prostr.2018.12.103

1. Introduction

Bioresorbable polymers are widely used for medical applications including fixation plates, screws, sutures and tissue-engineering scaffolds. Over the last decade, the use of 3D printing for medical research and clinical applications has grown significantly. It enables intricate porous geometries, important for scaffolds, to be produced that are not possible with conventional manufacturing processes. Due to the nature of 3D printing, anisotropic properties are observed in fabricated parts; the interface between 3D-printed layers has lower strength than that in other directions (Ahn 2003; Laureto 2018; Song 2017). There is a need for further understanding of failure mechanisms of such interfaces in order to improve the overall strength of 3D-printed parts.

The mechanical properties of 3D-printed parts are not well-understood at present. This is in part due to the complexity involved in 3D printing and the large number of controlled and uncontrolled variables that affect mechanical properties. These include: toolpath design, cooling rates of extrudates, travel speed of the printhead, time elapsed between extrusion of adjacent filaments, nozzle and printbed temperatures, filament size and shape, material formulation, etc. To reduce the complexity, a simple geometric design and printing strategy are required to ensure as many variables as possible remain constant at all positions within the 3D-printed tensile-testing specimen, as demonstrated in recent studies (Coogan 2017a, 2017b).

This paper presents a design and build strategy for an interfacial micro tensile-testing (IMTT) specimen, with the 3D-printer's extrusion rate controlled for each individual extruded filament to achieve a specimen with dogbone geometry. The design results in isolated individual interfaces between filaments, enabling precise control and characterisation of their geometry and mechanical performance. The applicability of results to medical polymers is discussed along with existing tensile-testing standards.

2. Methodology

IMTT specimens were produced using natural polylactide (3DXTECH® branded NatureWorks® polylactide 4043D, Sigma Aldrich) on an Ultimaker 2+ Extended system. Single filaments were extruded in a vertical stack normal to the print bed, as shown in Fig. 1. Machine control code (GCODE) was created using custom software to achieve precise control of the 3D-printer nozzle's path and extrusion rate. The width of filaments was varied from 0.6 to 0.9 mm (Fig. 1) by adjusting the extrusion rate of each filament; their height was 0.2 mm. A hollow box-shape (45 mm side-lengths and 38 mm height) was printed, as shown in Fig. 2, from which eight individual IMTT specimens (15 mm wide and 38 mm height) were cut with a blade. A 0.4 mm nozzle was used with a printhead's travel speed of 1000 mm min^{-1}. The nozzle temperature was set to 210°C and the print bed was heated to 60°C. Mechanical characterisation was performed on an Instron 3343 machine equipped with a 5 kN load cell at an extension rate of 2 mm min^{-1} until failure. Strength calculations used measurements with digital calliper of width and thickness. A Zeiss Primotech microscope was employed to characterise the geometry of the specimens.

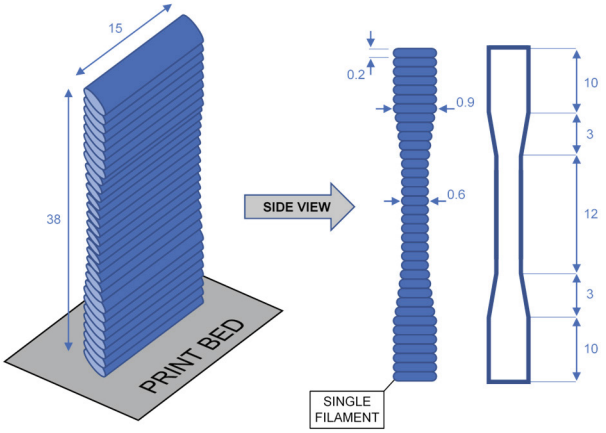

Fig. 1. The IMTT specimens were 3D-printed as a stack of individual filaments, normal to the print bed, with varying widths to achieve a dogbone cross section (all dimensions are in mm).

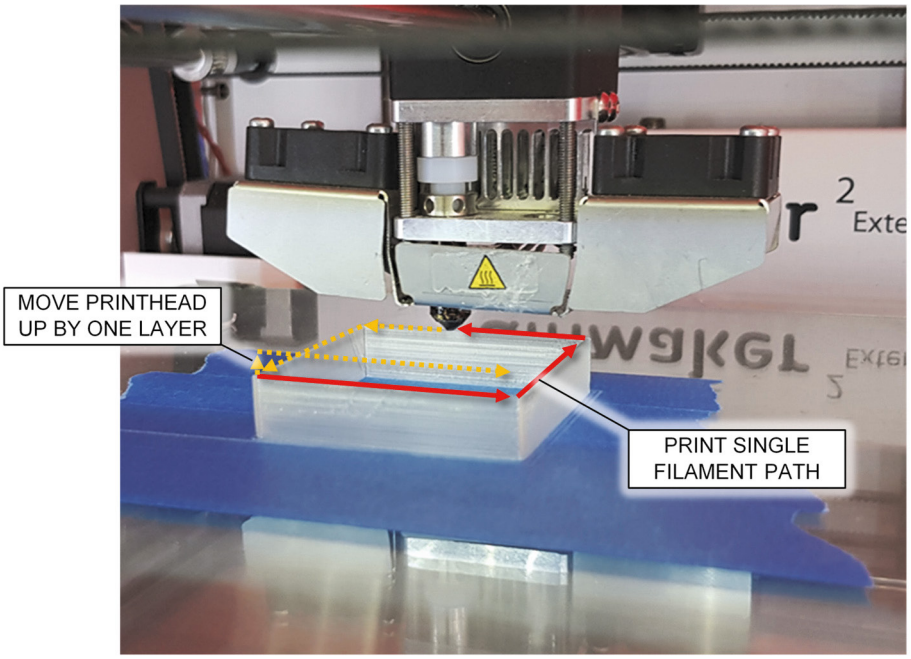

Fig. 2. The 3D printing process is shown with arrows to indicate nozzle movement. Solid red lines indicate previous nozzle's movement, dashed orange lines indicate its future movement on the current and subsequent layers.

3. Results and discussion

The results and discussion are split into three sections: the first section validates effective control of the 3D-printer's extrusion rate at different positions within the IMTT specimens to achieve the dogbone geometry indicated in Fig. 1; the second section demonstrates the mechanical performance of the specimens; and the third section considers the applicability of the method and specimen design to medical-grade materials.

3.1. Geometric characterisation

Preliminary trials with varying extrusion rates showed that filament widths ranging from approximately 0.3 to 1.2 mm were feasible. Below this range, filaments were printed with an inconsistent geometry and pores were present; above this range, feed-stock filament slipped in the feeding mechanism. The experimentally-achieved extrusion rate depended not only on its magnitude set in the GCODE, but also on nozzle temperature and the printhead's travel speed. Wider filaments were possible at higher nozzle temperatures (range from 190°C to 250°C was tested) and at lower travel speeds (range from 500 to 1500 mm min^{-1} was tested). For lower extrusion rates, nozzle temperature and the printhead's travel speed had lower, or negligible, impact on the actual extrusion rate. Slippage occurred in the feeding mechanism when the pressure within the melt chamber of the 3D-printer became high; it was due to higher polymer viscosity (at lower extrusion temperatures (Tian 2016)) and a faster extrusion (at higher travel speeds). Although not considered here, it is possible that the extrusion rate is also affected by other factors including the design of the 3D-printer, nozzle size, layer thickness and extrusion material.

A cross section of the neck-region of a 3D-printed IMTT specimen is shown in Fig. 3a; apparently, the filament widths increased from 611 to 820 µm across eleven layers. The width of the bond between filaments increased from 503 to 691 µm for the same section of the IMTT specimen (Fig. 3b). The bond was typically 100 to 130 µm narrower than the overall width of the filaments. The intended dogbone geometry, with a gradually increasing filament width, was successfully achieved by controlling the extrusion rate in the GCODE.

The overall width of filaments and bonds for the region between the grip sections of the IMTT specimen (ninety 3D-printed layers) is presented in Fig. 4 along with the designed width. The former correlated well with the designed width, and the latter was on average 114 µm narrower. Fluctuations between layers were small enough that the bond widths of the grip sections of specimens were always wider than those of the gauge section. In the gauge section of the IMTT specimen, the average bond width was 500 µm (range from 424 to 547 µm) and the average overall filament width was 608 µm (range from 532 to 641 µm) (see Fig. 4).

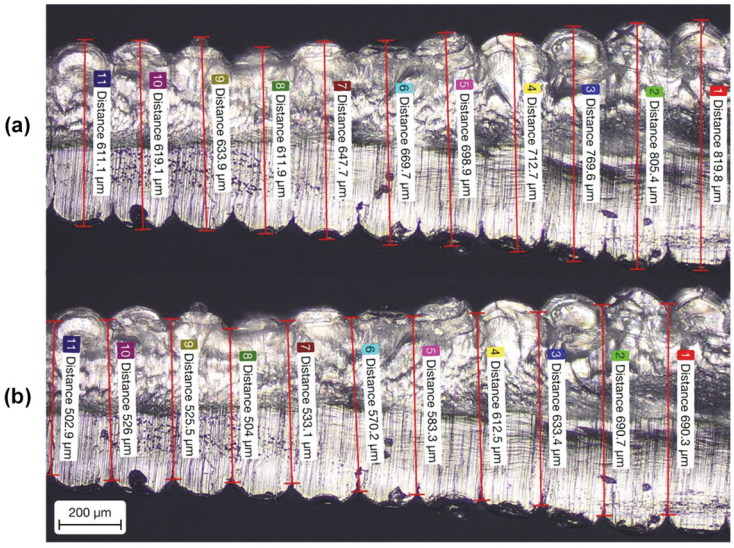

Fig. 3. The transition from narrower to wider filaments is shown with indicative measurements of overall width of filaments (a) and bonds (b).

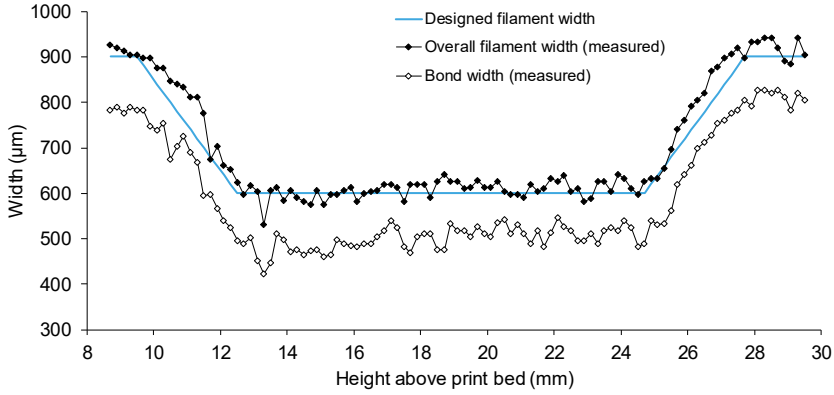

Fig. 4. Measurements for overall filament width (solid markers) and bond width (hollow markers) for the neck and gauge sections of one IMTT specimen. Designed filament width is also shown for reference (solid blue line).

3.2. Mechanical characterisation

Results of strength measurements for sixteen IMTT specimens are shown in Fig. 5a. Their average strength was 49.4 MPa (in a range from 21.0 to 61.1 MPa), which is comparable to values found in other studies for 3D-printed ASTM specimens (Laureto 2018; Song 2017; Spoerk 2017). The variation of strength between IMTT specimens is also comparable to that reported elsewhere for ASTM D638 type I and IV tensile-testing specimens (Laureto 2018). IMTT specimens typically failed along a single interface between two filaments, although in some cases the fracture was staggered across multiple interfaces. Fig. 5b demonstrates an example of a staggered fracture: the top and bottom fracture surfaces are shown for the same position of a fracture, which jumps from one interface to the neighbouring

interface for an approximately 1-mm-long section. A smooth and flat fracture surface (Fig. 5c) indicates brittle fracture (Xu 2014). Finer features towards the edges of fracture surface (top and bottom edges in Fig. 5c) may indicate a different fracture mechanism, potentially due to varying material properties near the surface as compared to the centre of filaments. Fracture mechanisms are the subject of our ongoing research

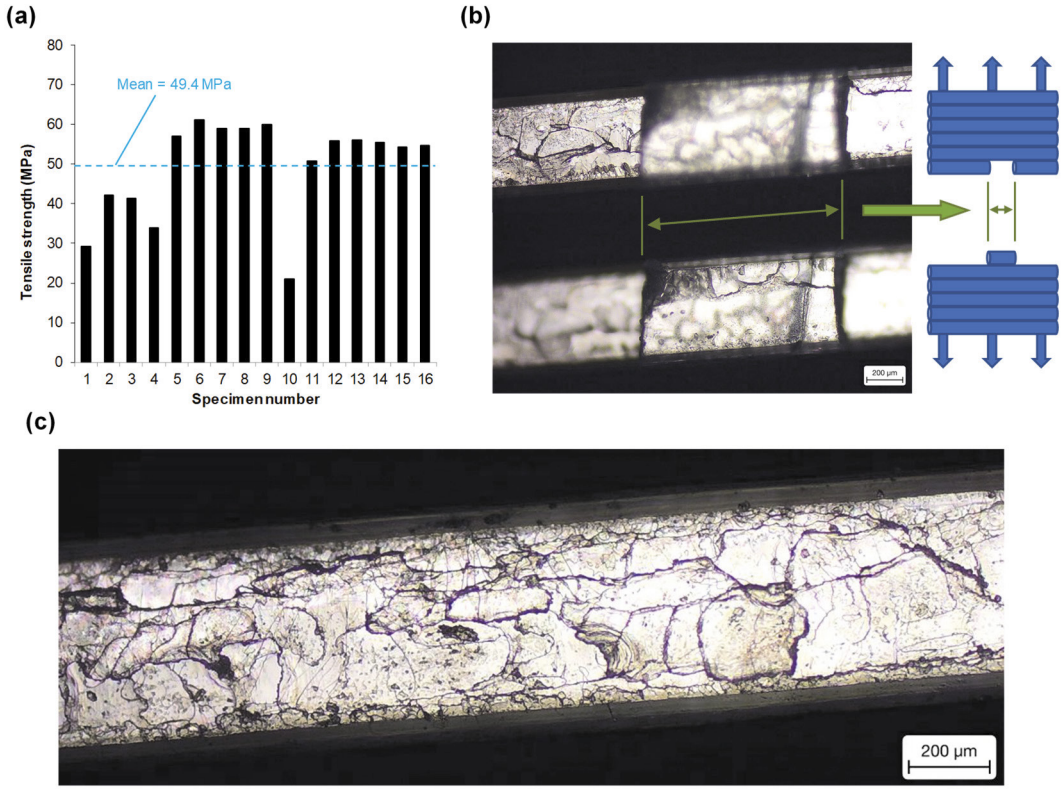

.

Fig. 5. (a) Tensile strength of sixteen specimens; (b) Staggered fracture across two interfaces; (c) Interfacial fracture surface.

3.3. Cost reduction

Time-series studies, such as mechanical degradation or biocompatibility assays, require multiple replicate specimens at several time intervals. When assessing the influence of multiple experimental variables, several hundred specimens may be required for a single study. Therefore, the cost of specimen material must be considered, along with costs associated with auxiliary equipment and consumables, such as storage vessels and cultivation medium, which must be regularly replenished. These are all affected by the volume of the specimens, which should be reduced where possible to diminish the cost of the study or to allow a greater number of experimental variables to be considered for the same cost.

The volumes of ASTM D638 type I, II, III, IV and V tensile-testing specimens are 8210, 6990 43400, 6340 and 1580 mm^3, respectively (Znanzhu 2017). The volume of ASTM D1708 micro tensile-testing specimens are 557 mm^3 and the IMTT specimen presented in this study had a volume of 446 mm^3. Medical-grade bioresorbable polymers costs from £19 to £175 per gram (quotations obtained from several companies Dec 2016 to Jul 2018). For an example material cost of £50 per gram, the ASTM D638 type I-V samples cost approximately £100 to £500 each, whereas the ASTM D1708 and IMTT specimens cost approximately £25 to £35 each.

The cost of IMTT specimens can be lowered further by additional reduction of their dimensions. The overall width of the IMTT specimen was set to 15 mm in this study. However, the gauge section of the D1708 specimen is only 5 mm wide; if this width was used for the IMTT specimen, an additional volume reduction of 67% could be achieved.

Furthermore, the width of filaments was set to between 0.6 and 0.9 mm; but this could also be reduced by 50%, based on our preliminary trials. Combining these modifications can reduce cost by 83% (to approximately £5 per specimen), and even greater cost reductions could be achieved if overall specimen length was reduced from 38 mm to around 10 mm, as used elsewhere for metal specimens (Rund 2015, Kumar 2014).

The total amount of polymer extruded per specimen was 620 mm^3, inclusive of waste created when cutting the eight samples from the hollow-box structure (shown in Fig. 2). Work is currently in progress to optimise the design and 3D printing strategy to further reduce polymer use and waste.

4. Conclusions

Micro tensile-testing specimens were 3D-printed by extruding filaments on top of each other in a single vertical stack (relative to a horizontal print bed). The extrusion rate of the 3D-printer was controlled to produce specimens with variable-width filaments resulting in a dogbone geometry profile, in which filaments were nominally 900 μm wide in the grip sections and 600 μm wide in the gauge section. The width of bonds between filaments was observed to be 114 μm narrower than the widest part of filaments on average. The ability to control extrusion rates of individual filaments resulted in a dogbone geometry achieved using the 3D-printer capabilities as opposed to custom dies or laser/waterjet cutting.

Average interfacial strength of the tested bioresorbable polymer was found to be 49.4 MPa, and its variation between specimens was comparable to that found elsewhere for 3D-printed ASTM D639 type I and IV samples. The fracture surface demonstrated brittle fracture of the interface between filaments. Custom control of the 3D-printer GCODE should be more prevalently used in future research to separate effects of individual experimental variables and develop greater understanding of properties of 3D-printed parts.

The micro tensile-testing specimens used an order of magnitude less polymer than D638 type I - IV specimens, which may equate to a cost savings of several hundred GBP per specimen for medical-grade bioresorbable polymer.

References

Ahn, S.H., Baek, C., Lee, S. and Ahn, I.S., 2003. Anisotropic tensile failure model of rapid prototyping parts-fused deposition modeling (FDM). International Journal of Modern Physics B, 17(08n09), pp.1510-1516.

Coogan, T.J. and Kazmer, D.O., 2017a. Bond and part strength in fused deposition modeling. Rapid Prototyping Journal, 23(2), pp.414-422.

Coogan, T.J. and Kazmer, D.O., 2017b. Healing simulation for bond strength prediction of FDM. Rapid Prototyping Journal, 23(3), pp.551-561.

Laureto, J.J. and Pearce, J.M., 2018. Anisotropic mechanical property variance between ASTM D638-14 type I and type IV fused filament fabricated specimens. Polymer Testing, 68, pp.294-301.

Kumar, K., Pooleery, A., Madhusoodanan, K., Singh, R.N., Chakravartty, J.K., Dutta, B.K. and Sinha, R.K., 2014. Use of miniature tensile specimen for measurement of mechanical properties. Procedia Engineering, 86, pp.899-909.

Rund, M., Procházka, R., Konopík, P., Džugan, J. and Folgar, H., 2015. Investigation of sample-size influence on tensile test results at different strain rates. Procedia Engineering, 114, pp.410-415.

Song, Y., Li, Y., Song, W., Yee, K., Lee, K.Y. and Tagarielli, V.L., 2017. Measurements of the mechanical response of unidirectional 3D-printed PLA. Materials & Design, 123, pp.154-164.

Spoerk, M., Arbeiter, F., Cajner, H., Sapkota, J. and Holzer, C., 2017. Parametric optimization of intra-and inter-layer strengths in parts produced by extrusion-based additive manufacturing of poly (lactic acid). Journal of Applied Polymer Science, 134(41), p.45401.

Tian, X., Liu, T., Yang, C., Wang, Q. and Li, D., 2016. Interface and performance of 3D printed continuous carbon fiber reinforced PLA composites. Composites Part A: Applied Science and Manufacturing, 88, pp.198-205.

Xu, H., Xie, L., Chen, J.B., Jiang, X., Hsiao, B.S., Zhong, G.J., Fu, Q. and Li, Z.M., 2014. Strong and tough micro/nanostructured poly (lactic acid) by mimicking the multifunctional hierarchy of shell. Materials Horizons, 1(5), pp.546-552.

Zhanzhu, 2017. Standard Tensile Test ASTM D638 Specimen Type I - V (1-5), accessed 25/07/2017, <www.thingiverse.com/thing:2332080>